Superfluidity, BEC, and dimensions of liquid ^{4}He in nanopores

L. Vranješ Markić[1] and H. R. Glyde[2]
[1]*Faculty of Science, University of Split, HR-21000 Split, Croatia, EU*
[2]*Department of Physics and Astronomy, University of Delaware, Newark, Delaware 19716-2593, USA*
(Received 22 April 2015; published 12 August 2015)

We present path integral Monte Carlo (PIMC) calculations of the superfluid fraction, ρ_S/ρ, and the one-body density matrix (OBDM) [Bose-Einstein condensation (BEC)] of liquid ^{4}He confined in nanopores. Liquid ^{4}He in nanopores represents a dense Bose liquid at reduced dimension and in disorder. The goal is to determine the effective dimensions of the liquid in the pores. It is to test whether observed properties, such as a very low onset temperature for superflow, T_c, can be predicted by a standard, static PIMC ρ_S/ρ. We simulate a cylinder of liquid of diameter d_L surrounded by 5 Å of inert solid ^{4}He in a nanopore of diameter d; $d = d_L + 10$ Å. We find a PIMC $\rho_S(T)/\rho$ and OBDM that scales as a 1D fluid Luttinger liquid at extremely small liquid pore diameters only, $d_L = 6$ Å. At this d_L, the liquid fills the pore in a 1D line at the center of the pore and there is no PIMC superflow. In the range $8 \leqslant d_L \leqslant 22$ Å the PIMC $\rho_S(T)/\rho$ scales as a 2D liquid. In this d_L range the liquid fills the pores in 2D-like cylindrical layers. The crossover from no superflow at $d = 16$ Å to superflow at $d \geqslant 18$ Å agrees with experiment. There is a crossover to 3D scaling at larger $d_L \simeq 22$ Å. In the range $8 \leqslant d_L \leqslant 22$ Å, the T_c predicted using the Kosterlitz-Thouless 2D scaling criterion of the OBDM agrees well with that obtained from $\rho_S(T)/\rho$. These results suggest that the superflow observed in small pore media is standard static superflow with the low T_c arising from its 2D character. An operational onset temperature, $T_{\rm BEC}$, for BEC can be defined as the temperature at which there is a crossover from exponential to algebraic decay in the OBDM. This definition leads to a $T_{\rm BEC} \geqslant T_c$ as observed in larger pore media.

DOI: 10.1103/PhysRevB.92.064510 PACS number(s): 67.25.dj, 67.25.dr, 67.10.Ba, 02.70.Ss

I. INTRODUCTION

Historically, superflow of liquid helium in porous media has been investigated as an integral part of superflow studies in bulk liquids [1]. In porous media, the critical temperature for the onset of superflow, T_c, is suppressed below the bulk liquid value, $T_\lambda = 2.17$ K at saturated vapor pressure (SVP). Generally, the smaller the pore diameter of the media, the further T_c is suppressed below T_λ. Similarly, the observed [1,2] superfluid critical exponent, v, of ρ_S/ρ below T_c, $\rho_S(T)/\rho = (1 - T/T_\lambda)^v$, generally differs somewhat from the bulk value ($v = 0.67$), except in Vycor where it is the same. Explanations of these different exponents have been proposed [3].

Recently, significantly smaller pore media have been investigated including measurements under pressure [4–12]. In these small pore media, T_c is suppressed to very low values, particularly under pressure. In 28 Å pore diameter FSM-16, as shown in Fig. 1 (top), $T_c \simeq 0.9$ K at SVP ($p \simeq 0$) and T_c drops to nearly 0 K under pressure [11]. In 25 Å mean pore diameter gelsil [7], T_c extrapolates to zero at 3.4 MPa. These very low T_c values appear to lie beyond the concepts that apply to larger pore media. Rather, it has been suggested that in small pore media there may be no static, zero frequency superfluidity at all and what is observed in torsional oscillators is an apparent, frequency dependent response characteristic of a 1D system [6,13–17]. Other properties, such as a specific heat that is linear in T at low temperature [4], suggest a fluid in pores with excitations that are "frozen out" perpendicular to the pore with phonons propagating in 1D along the pore only at low temperature. General arguments of why excitations in pores show 1D character and reviews of the 1D systems have been presented [18,19]. It is not clear at what pore diameters these arguments apply to superflow of ^{4}He in nanopores.

Bose-Einstein condensation (BEC) and phonon-roton (P-R) modes appear to be less modified by confinement than superfluidity [20–25]. Liquid ^{4}He supports well-defined P-R modes when there is BEC but not otherwise [20,26]. Measurements of P-R modes show that liquid ^{4}He in larger pore media and most small pore media supports well-defined modes up to T_λ. That is, $T_{\rm BEC} = T_\lambda$ in these media. For example, recent direct measurements of BEC and P-R modes in MCM-41 ($d = 47$ Å) show that both BEC and well-defined P-R modes exist up to T_λ in MCM-41 [see Fig. 1 (bottom)]. In the smaller pore FSM-16 shown in Fig. 1 (top), the onset temperature of both BEC, $T_{\rm BEC}$, and of well-defined modes may be suppressed somewhat below T_λ, but only somewhat. However, $T_{\rm BEC}$ is significantly higher than T_c and there is a temperature range in porous media, $T_c < T < T_\lambda$, where there is BEC but no superflow [21,22].

Adsorption isotherms of ^{4}He in porous media have been extensively measured [5,27]. These show that ^{4}He is highly attracted to the media walls. The initial ^{4}He entering the media is deposited on the walls. These initial layers are inert. Neutron scattering measurements indicate that the inert layers are chiefly amorphous solid helium [28]. In FSM-16, the inert layers are estimated to be an average of 5–6 Å thick [6,12]. Following the inert layers, the ^{4}He is deposited as liquid in the interior of the pore. In a wide variety of media a filling of $n_0 = 26$ μmol/m^2 of wall surface is needed before the onset of superflow is observed [1,29]. This is interpreted as the filling required to complete the inert layers and that the inert layers do not contribute to observable superflow. In fully filled media, the P-R mode energies of the liquid are the same as those in bulk liquid ^{4}He within precision. Since the mode energies are a sensitive function of the liquid density, this indicates that the density of the liquid in the pores is the same as the bulk density within precision. The picture is of 5–6 Å of "dead" layers on the walls, chiefly amorphous solid, with liquid in the center at or near bulk

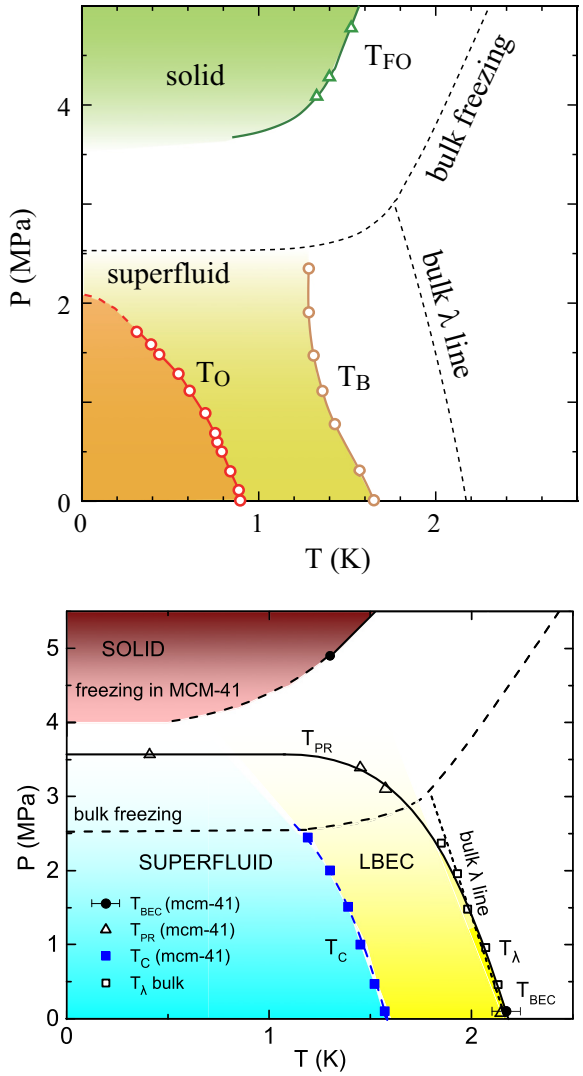

FIG. 1. (Color online) The phase diagram of ^{4}He confined in FSM (pore diameter $d = 28$ Å) (top) and in MCM-41 ($d = 45$ Å) (bottom) (from Refs. [11,20]). T_O (T_c) are the critical temperatures for superfluidity of liquid ^{4}He in the pores. T_λ is the corresponding temperature in the bulk liquid. T_B ($T_{\rm BEC}$) are the critical temperature for BEC in the pores. $T_{\rm PR}$ (triangles and solid line) in MCM-41 is the temperature at which the intensity in the P-R mode in the pores goes to zero. Within precision $T_{\rm PR} = T_\lambda$ for $p \leqslant 2.5$ MPa.

liquid density (at SVP). This picture is shown schematically in Fig. 2.

The porous media walls noted above are rough and irregular. This irregularity leads to a confining potential in the liquid that is disordered. Indeed ^{4}He in porous media is an example of bosons in disorder. For many properties it is not clear whether uniform confinement ignoring disorder is sufficient to reproduce observed behavior or whether the disordered nature of the confining potential must be explicitly incorporated.

In this context, we calculate the superfluid fraction, ρ_S/ρ, and the one-body density matrix (OBDM) of the liquid ^{4}He confined in pores of varying radii using path integral Monte Carlo (PIMC). The aim is to determine how T_c and ρ_S/ρ for superfluidity and $T_{\rm BEC}$ and the OBDM for BEC vary with pore radius of the liquid in the pore. A zero frequency $\rho_S(T)$ and

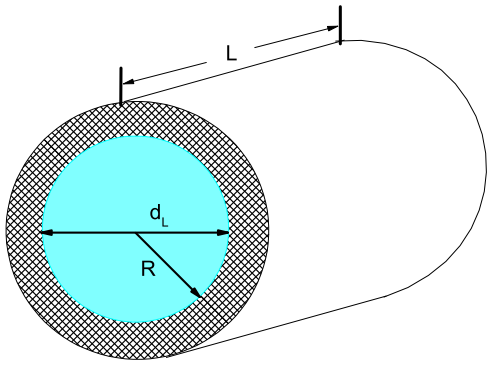

FIG. 2. (Color online) Model of ^{4}He in a nanopore of length L. The hatched area represents layers of "inert" ^{4}He attracted to the pore walls. The "inert" ^{4}He is estimated to be 1.5 layers or 5–6 Å thick [6,12]. The blue region is liquid in the interior that can support superflow and BEC. The liquid only is modeled in the present PIMC calculations. The liquid pore diameter is d_L (radius R). The corresponding nanopore diameter is estimated as $d \simeq d_L + 10$ Å.

T_c is calculated using PIMC. A key question is, how well can the observed $\rho_S(T)$ and T_c be reproduced by a zero frequency, PIMC $\rho_S(T)$? Can a T_c suppressed to very low temperature be obtained? Is a dynamical description needed and at what liquid radius? Is $T_{\rm BEC}$ for BEC less modified than T_c for ρ_S/ρ by confinement? What is the effective dimension of the confined liquid as a function of pore diameter inferred from $\rho_S(T)$, the OBDM, and direct calculations of the density, 3D, 2D, or 1D? Can we find a physical reason for this dimensionality? A final goal is to provide some indication of the impact of disorder on $\rho_S(T)$ and the OBDM.

II. MODEL OF HELIUM IN A NANOPORE AND PIMC

Our goal is to calculate ρ_S/ρ and the OBDM of liquid ^{4}He in the interior of nanopores. As shown in Fig. 2 and discussed above, the interior walls of a pore are coated with layers of inert ^{4}He, chiefly in the form of amorphous solid ^{4}He. The inert layers on the walls of FSM-16 are estimated [5,12] to be 5 Å thick. In the interior of the nanopore is a cylinder of liquid ^{4}He at or close to bulk liquid density confined by the inert solid and the nanopore walls. To reduce the system size, we assume that the inert layers do not contribute to superflow at all. We have simulated only the liquid in the interior of a pore, a cylinder of liquid confined to a radius, R, by the inert layers and pore walls. The nanopore diameter corresponding to R is $d = 2R + 10$ Å. A confining potential arising from the inert layers and the pore medium is employed.

Specifically, we simulate liquid ^{4}He confined in a nanopore described by the Hamiltonian,

$$\hat{H} = -\frac{\hbar^2}{2m}\sum_{i=1}^{N}\Delta_i + \sum_{i<j}^{N} U(r_{ij}) + \sum_{i=1}^{N} V(\rho_i), \qquad (1)$$

where N is the number of ^{4}He atoms of mass m, Δ is the Laplacian, $U(r)$ is the interaction between ^{4}He atoms represented by the Aziz potential [30], and $V(\rho)$ is the confining potential at a distance ρ from the center of the pore. A confining potential arising from a cylindrical pore

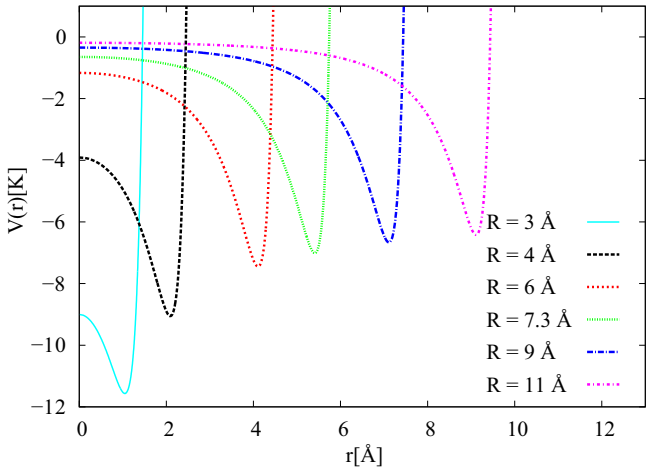

FIG. 3. (Color online) Confining potentials seen by the liquid in the pore as a function of liquid pore radius R. The magnitude of the confining potential is adjusted to have liquid in the pores at (or close to) bulk liquid density ($\rho = 0.0219$ Å^{-3}).

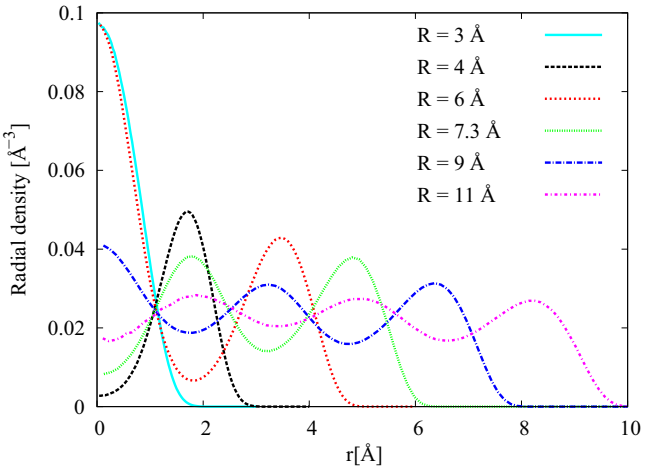

FIG. 4. (Color online) Radial density profile $\rho(r)$ of liquid in nanopores for liquid pore radii $R = 3$–11 Å. The temperature is $T = 1$ K except at $R = 11$ Å where $T = 1.5$ K.

(hole) in an infinite medium was used [31]. The potential form results from the integration of the Lennard-Jones pair potential between ^{4}He and the pore wall atoms over the volume of the pore media. The media is assumed to be comprised of a set of concentric cylindrical surfaces of infinite length, and radius ρ_s, as described in Ref. [31]. If atoms are smeared continuously over the medium with number density n, the potential is

$$V(\rho) = 3\epsilon n\pi\sigma^6 \int_R^{R_i} \rho_s d\rho_s \int_0^{\pi} d\phi_s \times \left[\frac{21}{32}\frac{\sigma^6}{\left(\rho^2+\rho_s^2-2\rho\rho_s\cos\phi_s\right)^{11/2}} - \frac{1}{\left(\rho^2+\rho_s^2-2\rho\rho_s\cos\phi_s\right)^{5/2}}\right], \quad (2)$$

where the medium extends from R, the radius of the liquid, to R_i. Equation (2) is integrated numerically up to $R_i = 3R$.

Our pore media consists of two layers of inert solid helium (5 Å thick) followed by standard nanopore media. The hard core parameter σ remains well determined since both ^{4}He and the media atoms have a hard core. However, the attractive part will be different from the case of pure pore media throughout. We have chosen potential parameters in $V(\rho)$ so that the helium in the interior of the pore, $r < R$, remains liquid: $\sigma = 2.2$ Å, $\epsilon = 3$ K, and $n = 0.078$ Å^{-3}, where ϵ is not well known. The resulting interaction has a steep hard core and shallow attractive minimum near the pore wall as shown in Fig. 3. The $\rho_S(T)/\rho$ is determined almost entirely by the hard wall radius R relative to the hard core diameter of the ^{4}He atom. It is quite insensitive to ϵ, as discussed in full in Sec. IV. The same form of confining potential, with parameters appropriate for Si_3N_4, has been used in Refs. [15,16,32].

The calculations were performed using the finite-temperature worm algorithm path integral Monte Carlo [33,34]. We are indebted to M. Boninsegni who provided the code. The canonical version of the code with the fixed number of particles, N, was used. The discretized imaginary time $\delta\tau = 0.004$ K^{-1}. We verified that the bias coming from the use of finite $\delta\tau$ is below the statistical noise. Periodic boundary conditions were used along the length of the pore.

Figure 4 shows the density profiles of the liquid ^{4}He in the pores as a function of the liquid pore radius, R. For a very small radius, $R = 3$ Å, the liquid is confined to the center of the pore with the maximum in density at the center of the pore (1D). At larger R, there are oscillations in the density as a function of the distance r from the center of the pore. The maxima of density in these oscillations are generally displaced from the center of the pore, even at $R = 4$ Å, showing that the liquid is deposited in cylindrical layers [32,35–37]. The oscillations are created by the hard wall [35] at R which leads to oscillations familiar in the pair correlation function appearing in the density. As R increases, the magnitude of the oscillations decrease. At $R = 11$ Å, the magnitude is small, layering is less pronounced, and the liquid is closer to a uniform bulk liquid (3D).

In a bulk liquid, the density is $\rho = N/V$. In a finite-size system, there are finite-size effects. Specifically, because of the hard core of the helium potential, a helium atom cannot occupy the space immediately adjacent to a hard wall. The volume within approximately 1 Å is excluded (see density profiles in Fig. 4). To determine the liquid density in pores we have taken account of this excluded volume and reduced the volume available to the liquid to $V' = \pi(R')^2 L$ where $R' = R - 1$ Å. The density we have used is therefore $\rho' = N/V'$. The ρ' were selected to be close to bulk liquid density, 0.0219 Å^{-3} at SVP (see Table I).

III. RESULTS

A. Superfluid density

In Fig. 5 we show the broad features of the PIMC superfluid fraction, $\rho_S(T)/\rho$, in a nanopore of length $L = 60$ Å. The $\rho_S(T)/\rho$ was calculated using the winding number estimator [38,39]. The $\rho_S(T)/\rho$ moves to lower temperature and the shape changes as the radius R of the cylinder of liquid in the nanopore is reduced from $R = 11$ to 3 Å. The average liquid density in the cylinder of liquid, ρ', is given in Table I. The corresponding nanopore diameter, d, is $d = 2R + 10$ Å.

TABLE I. Data of eight samples of liquid ^{4}He in a nanopore of length $L = 60$ Å : number of particles N, liquid radius R, density ρ, effective liquid radius R' (estimated from the radial density profile), and effective density ρ'. The bulk liquid density at SVP is 0.0219 Å^{-3}. At densities 0.0241 Å^{-3} and 0.0160 Å^{-3}, the bulk liquid pressure is approximately 13 bars and −9 bars, respectively.

N	R (Å)	$\rho = N/(R^2\pi L)$ (Å^{-3})	R' (Å)	$\rho' = N/(R'^2\pi L)$ (Å^{-3})
16	3	0.0094	2	0.0212
36	4	0.0119	3	0.0212
100	6	0.0147	5	0.0212
120	7.3	0.0120	6.3	0.0160
160	7.3	0.0159	6.3	0.0214
180	7.3	0.0179	6.3	0.0241
240	9	0.0157	8	0.0199
360	11	0.0158	10	0.0191

The $\rho_S(T)/\rho$ goes to 1 at low temperature as in the bulk liquid because the nanopore is straight and has smooth walls. There is no tortuosity. At $R = 11$ Å ($d = 32$ Å) the shape of $\rho_S(T)/\rho$ is similar [34] to that of bulk liquid ^{4}He. The $\rho_S(T)/\rho$ goes to zero at a temperature (T_c) somewhat below the bulk liquid critical temperature, $T_\lambda = 2.17$ K at SVP. Finite-size (finite-L) effects create a tail to ρ_S/ρ extending it to higher temperatures above T_c. As the liquid pore radius R is reduced, T_c moves to lower temperatures. The shape of $\rho_S(T)/\rho$ is especially different at $R = 3$ Å. The change in shape reflects the change in effective dimensions of the liquid in the nanopore, going from 3D to 2D to 1D, as R is reduced. The liquid has predominantly 2D character in the range $6 < R < 11$ Å and 1D at $R = 3$ Å, as we show below on the basis of scaling properties. There is no superflow at 1D.

Figure 6 shows the PIMC $\rho_S(T)/\rho$ versus temperature in a nanopore of liquid pore radius $R = 7.3$ Å at three liquid densities and several pore lengths L. The aim is to reveal the density dependence and display finite-size effects. The middle frame shows ρ_S/ρ at density $\rho' = 0.0214$ Å^{-3} which is close to the bulk liquid density at SVP. Finite-size effects are significant. As shown below, the T_c can be identified as the temperature T at which the $\rho_S(T,L)/\rho$ for different L cross. This indicates a $T_c \simeq 1.2$ K at $\rho' = 0.0214$ Å^{-3}. T_c is suppressed substantially below $T_\lambda = 2.17$ K by confinement, demonstrating that a T_c substantially below T_λ can be obtained from a static, PIMC ρ_S/ρ. At higher density $\rho' = 0.0241$ Å^{-3} T_c is suppressed to still lower temperature, $T_c \simeq 0.9$ K. This shows qualitatively that T_c decreases as density is increased as is observed [7,11]. In bulk ^{4}He the pressure at density 0.0241 Å^{-3} is 13 bars. At the solidification line, $p = 25.3$ bars, the bulk liquid density is $\rho = 0.0262$ Å^{-3}.

To identify the effective dimensions of the confined liquid, we use the scaling properties of $\rho_S(T,L)/\rho$. For 2D and 3D,

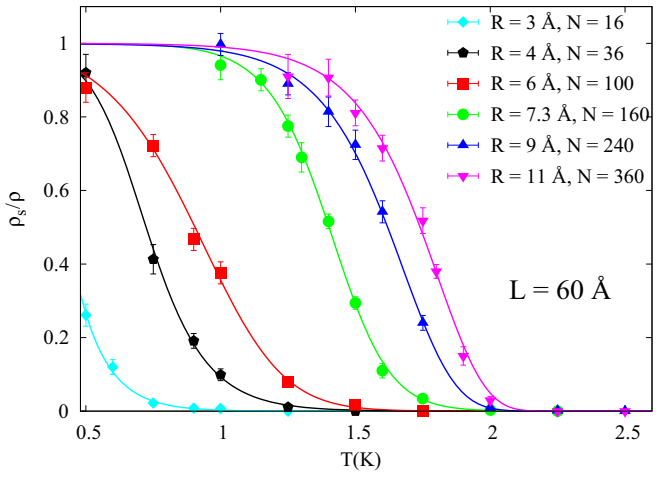

FIG. 5. (Color online) Superfluid fraction, $\rho_S(T)/\rho$, of liquid ^{4}He versus temperature for liquid pore radii $R = 3$–11 Å and pore length $L = 60$ Å. N is the number of particles in the pore. The $\rho_S(T)/\rho$ moves to lower temperature as R decreases. At $R = 3$ Å, the apparent ρ_S/ρ is only a finite-size effect. The corresponding nanopore diameter is $d \simeq 2R + 10$ Å.

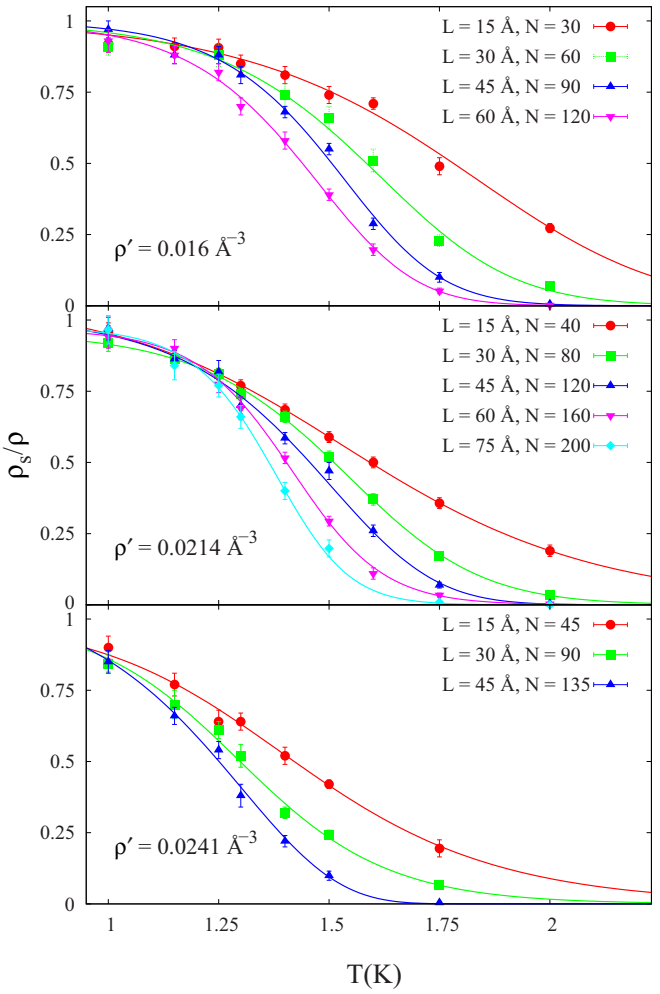

FIG. 6. (Color online) Superfluid fraction, $\rho_S(T)/\rho$, versus temperature for a fixed liquid pore radius $R = 7.3$ Å and varying pore length L and density. From top to bottom, selected densities correspond to pressures in the bulk liquid of −9 bars, −2 bars, and 13 bars. The legend shows the pore length, L, and number of particles, N. The superfluid fraction moves to lower temperature as the pore length, L, and density increase.

the central assumption is that intensive quantities such as ρ_S/ρ depend on L only through ratio L/ξ where ξ is the correlation length [40,41]. Since the temperature dependence of ξ is $t^{-\nu}$, where $t = (T - T_c)/T_c$ and ν is the correlation length exponent near T_c, this means that $L/\xi \sim Lt^{\nu} \sim (L^{1/\nu}t)^{\nu}$. Thus ρ_S/ρ depends on the "scaling" variable $y = (L^{1/\nu}t)$ rather than separately on L and T. Also near T_c, $\rho_S(T)/\rho \sim t^{\upsilon}$ (at constant L), where υ is the superfluid density exponent. Converting this to a function of L through the scaling variable, we have

$$\rho_S(T,L)/\rho = L^{-\frac{\upsilon}{\nu}} f(L^{1/\nu}t). \tag{3}$$

A simple choice of $f(y)$ is $f(y) = my + b$.

The scaling relation depends on dimensions through the Josephson hyperscaling relation $\upsilon = (D-2)\nu$, where D is the dimension. In 2D $\upsilon = 0$ and

$$\rho_S(T,L)/\rho = m(L^{1/\nu}t) + b. \tag{4}$$

An important corollary of this relation is that at $T = T_c$ ($t = 0$), $\rho_S(T,L)/\rho = b$ is independent of L. T_c can be identified as the temperature at which $\rho_S(T,L)/\rho$ is the same for all L.

Figure 7 shows $\rho_S(T)/\rho$ for four liquid pore radii $R =$ 6–11 Å and several lengths L of the nanopore. In 2D we estimate the critical temperature and the correlation length exponent as the parameters for which we get best linear fit to Eq. (4). The values of T_c so obtained, which are listed in Table I, also agree very well with the temperatures at which the $\rho_S(T)/\rho$ curves cross. At $R = 7.3$ Å, for example, this gives $T_c = 1.21$ K.

In Fig. 8 the $\rho_S(T,L)/\rho$ for $R = 7.3$ Å and $R = 9$ Å are plotted versus the scaling variable $y = L^{1/\nu}t$. We see that $\rho_S(T,L)/\rho$ indeed scales with $L^{1/\nu}t$ as predicted by Eq. (4). Both Figs. 7 and 8 show the character expected for a 2D fluid: the $\rho_S(T)/\rho$ for different L cross at a single temperature in Fig. 7 and ρ_S/ρ scales with $y = L^{1/\nu}t$ in Fig. 8. For $R = 4$–11 Å, the liquid ^{4}He in the nanopore responds like a 2D fluid. We attribute this to the He being deposited in cylindrical layers in the nanopore with clear minima in the density between the layers.

For 3D the scaling Eq. (3) is $L\rho_S(T,L)/\rho = mL^{1/\nu}t + b$. Figure 9 (top) shows $\rho_S(T)/\rho$ at $R = 11$ Å scaled according to both the 2D and 3D scaling relations. The $L^{\frac{\upsilon}{\nu}}\rho_S(T)/\rho$ scales with $y = (L^{1/\nu}t)$ equally well as a 2D or 3D fluid. In Fig. 9 (bottom) $L\rho_S(T,L)/\rho$ versus T for different L cross at a common temperature (T_c) as expected for a 3D fluid. Comparing the bottom of Figs. 7 and 9, we see the $\rho_S(T)/\rho$ at $R = 11$ Å crosses at a common temperature equally well when scaled as a 2D or 3D fluid. The amplitude of the oscillations in the liquid density shown in Fig. 4 is smaller at $R = 11$ Å and the liquid is approaching a uniform density as in a bulk 3D liquid. This suggests a crossover from 2D to 3D at or near $R = 11$ Å ($d = 32$ Å). The best-fit 3D exponent $\nu = 0.69(1)$ for $R = 11$ Å is also consistent with the bulk 3D liquid value $\nu = 0.67$ (in 3D, $\nu = \upsilon$), within precision. The exponent ν in 3D helium separated by weak links has recently been investigated [42].

Figure 10 shows $\rho_S(T)/\rho$ for liquid pore radii $R = 3$ Å and 4 Å. Shown is $\rho_S(T,L)/\rho$ as a function of temperature for nanopore lengths $L = 15$–60 Å. The temperature dependence of ρ_S/ρ at $R = 3$ and 4 Å are quite different from each other. At $R = 3$ Å, the ρ_S/ρ gets systematically smaller at

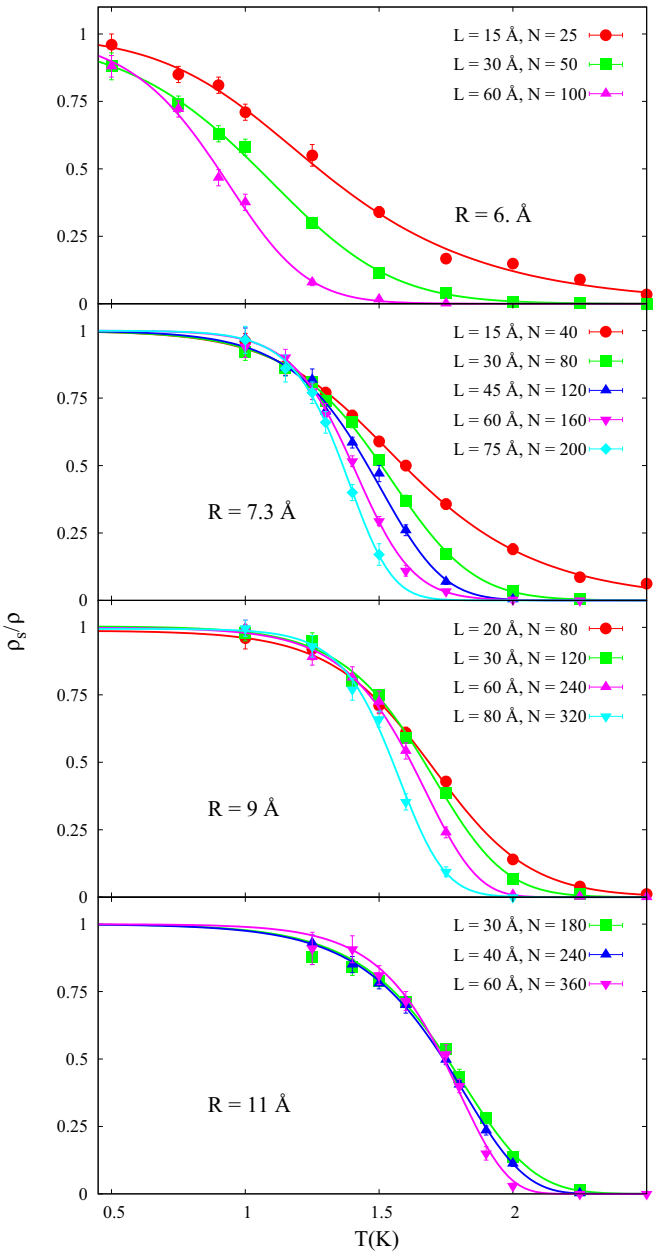

FIG. 7. (Color online) Superfluid fraction, $\rho_S(T)/\rho$, for liquid pore radii $R = 6$–11 Å. In the legend is the pore length L and number of particles N. At $R = 7.3$ and 9 Å, $\rho_S(T)/\rho$ scales like a 2D liquid. In 2D $\rho_S(T)/\rho$ for different L cross at $T = T_c$ indicating $T_c \simeq 1.2$ and 1.4 K at $R = 7.3$ and 9 Å. A $T_c < 0.5$ K is indicated at $R = 6$ Å. At $R = 11$ Å, $\rho_S(T)/\rho$ scales equally well as a 2D or 3D liquid.

low temperature as L increases as if it goes to zero at $L = \infty$. There is no apparent transition to a superfluid state [no crossing of $\rho_S(T,L)/\rho$ for different L at temperature T_c]. In contrast, at $R = 4$ Å, $\rho_S(T,L)/\rho$ goes to unity at low T independent of L. Below we show, based on the scaling character of $\rho_S(T,L)/\rho$, that the liquid at $R = 3$ Å responds like a 1D liquid while that at $R = 4$ Å does not.

Low energy, long wavelength density response in a 1D Bose liquid can be described [43,44] by the Luttinger liquid (LL) Hamiltonian [45]. LL theory predicts an apparent superfluid

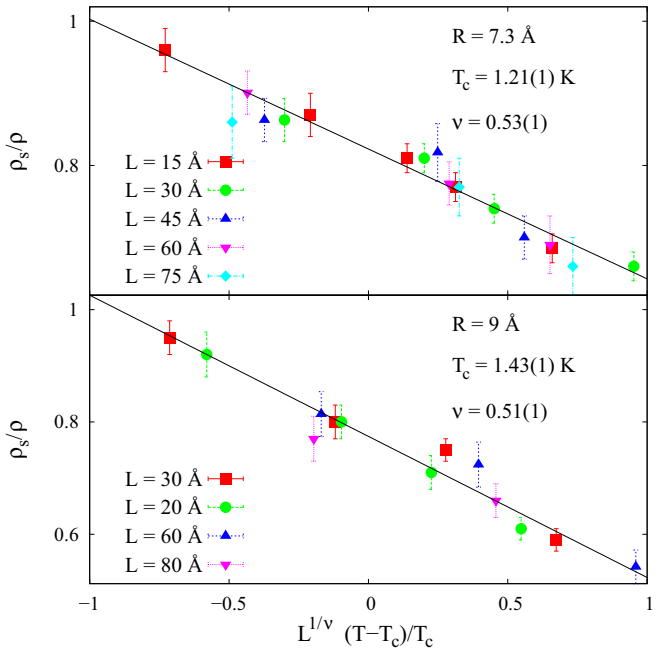

FIG. 8. (Color online) Finite-size scaling of $\rho_S(T)/\rho$ for $R = 7.3$ Å and 9.0 Å, assuming two-dimensional (2D) scaling.

density calculated from the winding number of [14,15]

$$\rho_S(T,L)/\rho = 1 - \frac{\pi}{u}\left|\frac{\Theta_3''(0,e^{-2\pi u})}{\Theta_3(0,e^{-2\pi u})}\right|, \qquad (5)$$

where $u = L/(\hbar\beta v_J)$, $\beta = 1/k_BT$ is the inverse temperature, L is the nanopore length, and $v_J = K/v_S$ is a constant that depends on the Luttinger liquid parameter, K, and the velocity, v_S, of the density modes [18,19,43,46]. For a Galilean invariant Bose system, v_J reduces to $v_J = \pi\hbar\rho_0/m$ where $\rho_0 = N/L$ is the 1D linear density. In this case $v_J = v_F$, where v_F is the Fermi velocity of a 1D spinless Fermi gas at the same density ρ_0. $\Theta_3(z,q)$ is the Jacobi Theta function and $\Theta_3'' = d^2\Theta_3/dz^2$. For the present purposes, if the ^{4}He responds like a 1D LL harmonic fluid, $\rho_S(T,L)/\rho$ will depend only on the single "scaling" variable $u = L/(\hbar\beta v_J)$ and not independently on $\beta = 1/k_BT$ and L. Essentially, we identify the confined fluid as 1D-like if ρ_S/ρ "scales" as u and satisfies Eq. (5).

From Fig. 11, we see that at $R = 3$ Å the PIMC ρ_S/ρ depends solely on $L/(\hbar\beta v_J)$. Values of $\rho_S(T,L)/\rho$ obtained from a spectrum of values of T and L collapse onto a single line. The line is well fitted by Eq. (5) with v_J as an adjustable parameter. The ρ_S/ρ has the character of a 1D fluid. Specifically, there is no static, zero frequency superfluidity. The apparent finite ρ_S/ρ at $R = 3$ Å is a finite-size effect and $\rho_S/\rho \to 0$ as $L \to \infty$. This is a physically reasonable result since at $R = 3$ Å, the liquid density peaks at the center of the pore. The ^{4}He lies in a 1D line along the pore. This can be seen in Fig. 4 and from the bottom of Fig. 11. It is 1D because the hard core diameter $\sigma = 2.56$ Å of the ^{4}He is too large to allow two ^{4}He atoms to lie across a confining radius $R = 3$ Å without penetrating the hard core of the confining potential. The v_J can also be obtained directly from $\hbar v_J = \pi(\hbar^2/m)\rho_0$. The linear density of the present 1D system at $R = 3$ Å is $\rho_0 = N/L = 1/3.75$ Å^{-1} (see Fig. 10).

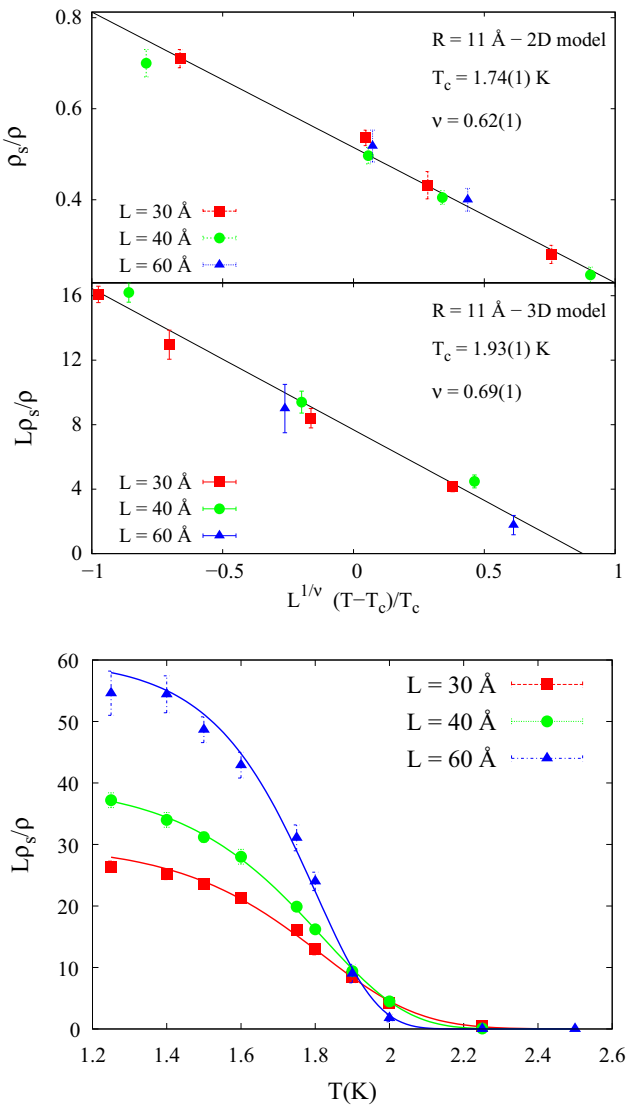

FIG. 9. (Color online) Top: Finite-size scaling of $\rho_S(T)/\rho$ for $R = 11$ Å, assuming 2D and 3D scaling. Bottom: $L\rho_S(T)/\rho$ vs temperature. For scaling as a 3D fluid, $L\rho_S(T)/\rho$ for different L cross at the same temperature, T_c.

This gives $\hbar v_J = 10.2$ Å K. The fitted value 10.4 Å K that collapses the superfluid densities onto a single line in Fig. 11 agrees well with the anticipated value of 10.2 Å K assuming Galilean invariance.

In contrast, as seen from Fig. 12, $\rho_S(T,L)/\rho$ at $R = 4$ Å does not scale as predicted by 1D LL theory. Similarly, as seen from the bottom of Fig. 12, the ^{4}He density is not at the center of the pore in a 1D line. Rather, the density lies in a cylindrical layer (2D) with a surface on each side of the layer, inside and outside the cylinder of liquid. Also, the shape of $\rho_S(T)/\rho$ in Fig. 10 at $R = 4$ Å indicates a very low but finite T_c ($T_c \leqslant 0.4$ K) as expected for a 2D fluid. Thus, there is a crossover from 1D behavior at $R = 3$ Å to clear 2D behavior at $R = 4$ Å. In the range $4 \leqslant R \leqslant 11$ Å the confined liquid shows 2D character (except at $R = 6$ Å).

At $R = 6$ Å, there is a mixture of 1D and 2D response since at $R = 6$ Å part of the density lies at the center of the pore

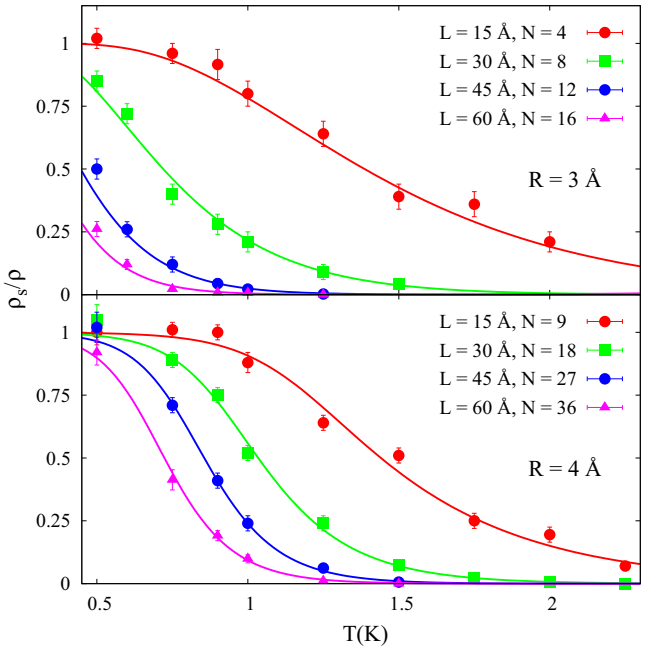

FIG. 10. (Color online) Superfluid fraction, $\rho_S(T)/\rho$, for liquid pore radii $R = 3$ Å and 4 Å. In legend is the nanopore length L and the number of ^{4}He atoms N. At $R = 3$ Å, $\rho_S(T)/\rho$ scales as a 1D liquid, at $R = 4$ Å as a 2D liquid.

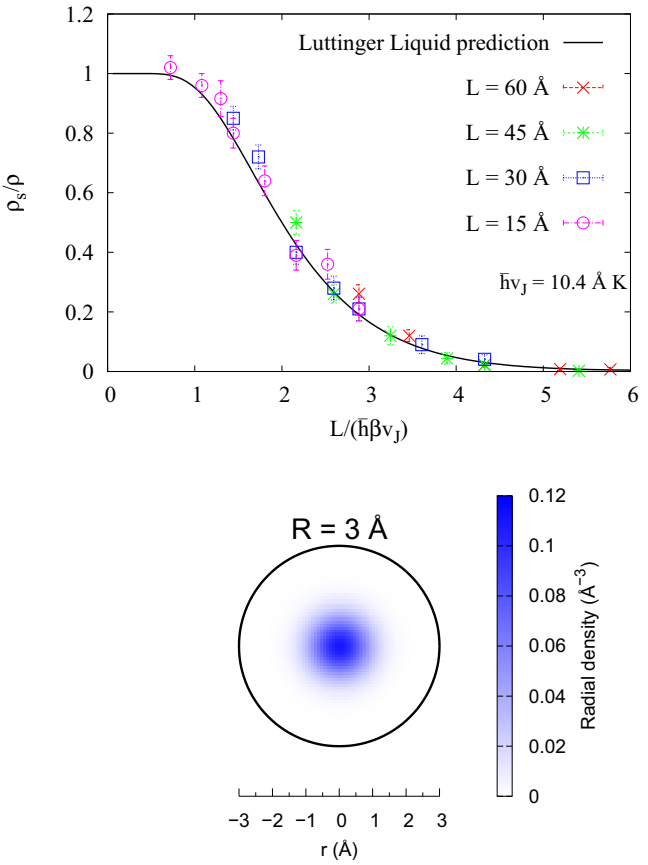

FIG. 11. (Color online) Top: Scaling of $\rho_S(T)/\rho$ at $R = 3$ Å vs $L/(\hbar\beta v_J)$ for different temperatures T ($\beta = k_B T$) and pore lengths L. The solid line is the Luttinger liquid (LL) prediction. Bottom: The density profile of liquid ^{4}He in the nanopore showing that liquid lies at the center of the pore in a 1D line of atoms along the pore.

as in a 1D liquid, as seen in Fig. 4. The 1D portion does not contribute to ρ_S/ρ. This would explain the large drop in ρ_S/ρ between $R = 7.3$ Å and $R = 6$ Å seen in Fig. 5 and the large apparent finite-size effects seen at $R = 6$ Å in Fig. 7.

Figure 13 (top) compares the $\rho_S(T)/\rho$ calculated using the winding number and area estimator methods for a liquid pore radius $R = 7.3$ Å and nanopore length $L = 60$ Å. The two agree well at low temperature, both predicting a $\rho_S(T)/\rho$ that goes to 1. However they differ significantly at higher temperature. An important difference between the two is that area estimator $\rho_S(T)/\rho$ has a finite-size effect that is independent of the length L of the nanopore. As seen in Fig. 13 (bottom) the area estimator ρ_S/ρ is independent of L. In contrast the winding number $\rho_S(T)/\rho$ is very sensitive to L, as seen in Fig. 7. The two would agree much better had we chosen to compare the two for $L = 15$ Å rather than $L = 60$ Å. Within these differences, the two methods are consistent because they predict within the error bars the same values below T_c. The area estimator is further discussed in Refs. [15,16,32].

B. One-body density matrix

In this section we present PIMC calculations of the one-body density matrix (OBDM), $n(z)$, of liquid ^{4}He in nanopores for distances z along the pore. The goal is (1) to infer the effective dimensions of the confined liquid as a function of pore diameter from the character of $n(z)$, (2) to determine an apparent onset temperature for BEC, $T_{\rm BEC}$, in confined liquid ^{4}He, one that could be observed in the same way that $T_{\rm BEC}$ is observed in bulk systems, and (3) to obtain the onset temperature, T_c, for superfluidity from the OBDM following the method proposed by Kosterlitz and Thouless [47].

The OBDM is defined as $n(\mathbf{r}_1,\mathbf{r}'_1) = \langle\psi^\dagger(\mathbf{r}_1)\psi(\mathbf{r}'_1)\rangle$, the probability amplitude for annihilating a ^{4}He atom at $\mathbf{r}'_1$ and creating one at $\mathbf{r}_1$. In a homogeneous system it depends only on the distance between the atoms $r = |\mathbf{r}_1 - \mathbf{r}'_1|$. The $n(r)$ is the Fourier transform of the atomic momentum distribution, $n(k)$. Since we were interested in the long-range behavior of the OBDM, we averaged over the coordinates perpendicular to the axis of the nanopore, and thus obtained a $n(z)$ which depends only on the separation of the atoms along the pore, $z = |z_1 - z'_1|$.

At small r ($r \leqslant 2.5$ Å), $n(r)$ is approximately a Gaussian. This follows because the atomic momentum distribution is approximately a Gaussian in 1D, 2D, and 3D (with some observable deviations). At larger r, $r \geqslant 2.5$ Å, in normal liquids (no BEC), $n(r)$ decays exponentially with increasing r in 3D and 2D. In 1D $n(z)$ is predicted to decay algebraically with z at large z. In contrast, in a 3D bulk fluid at low temperature, $T \leqslant T_\lambda$, where there is BEC, $n(r)$ at large r ($r \geqslant 3$ Å) goes to a constant, $n(r) = n_0$, where $n_0 = N_0/N$ is the BEC condensate fraction. In a 2D fluid at low temperature, $n(r)$ at large r decays algebraically with increasing r rather than exponentially. Indeed as T is decreased, the height of the tail in $n(r)$ increases in magnitude and the tail extends to longer distances. At $T = 0$ K, the algebraic decay becomes

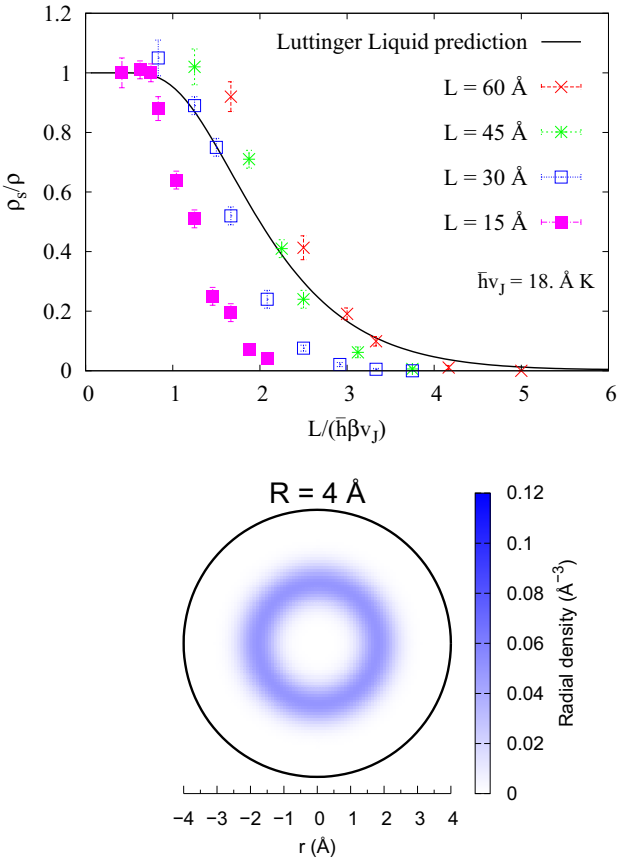

FIG. 12. (Color online) As Fig. 11 for $R = 4$ Å. At $R = 4$ Å, ρ_S/ρ does not fulfill LL scaling. The density profile (bottom) shows that the liquid lies in a cylindrical layer (2D) along the pore.

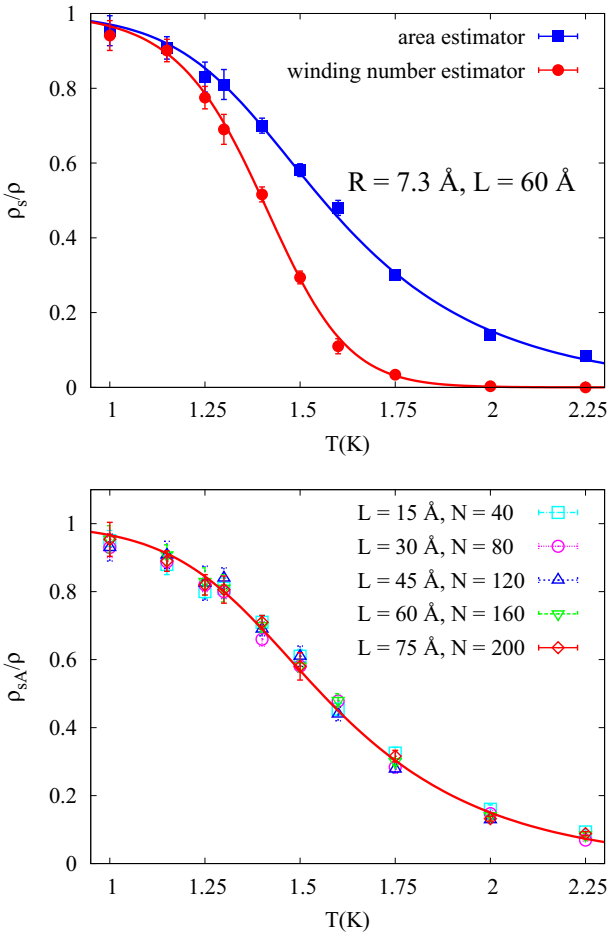

FIG. 13. (Color online) Top: Comparison of winding number and area estimator of $\rho_S(T)/\rho$ for pore liquid radius $R = 7.3$ Å and length $L = 60$ Å. Bottom: Area estimator of $\rho_S(T)/\rho$ vs temperature for several pore lengths L.

a constant as in 3D and a condensate fraction can be clearly defined.

Figure 14 shows the OBDM of liquid ^{4}He in nanopores at four liquid pore radii, $6 \leqslant R \leqslant 11$ Å. At these pore radii, the OBDM of the confined liquid has the character of a 2D liquid. At small z, $z \lesssim 3$ Å, $n(z)$ is approximately Gaussian in z. At high temperature, e.g., at $T = 2.25$ K for $R = 11$ Å, $n(z)$ for $z \gtrsim 3$ Å decays exponentially over 2–3 orders of magnitude within statistical fluctuations. As T is decreased, we see a crossover from exponential to algebraic decay characteristic of 2D. The algebraic decay may be represented approximately by $n(z) \simeq z^{-\eta(T)}$, where $\eta(T)$ is a temperature dependent constant.

As an operational definition, we define $T_{\rm BEC}$ in 2D as the temperature at which the crossover from exponential to algebraic decay of $n(z)$ takes place. This definition is pragmatic in the sense that this crossover can be observed [48] in 2D using the same techniques used to measure n_0 in 3D liquid ^{4}He. The definition also coincides with the definition of $T_{\rm BEC}$ in 3D. This definition and Fig. 14 lead to the values of $T_{\rm BEC}$ for confined ^{4}He shown in Table II.

As temperature is lowered still further, the magnitude of the algebraic tail in $n(z)$ increases and the tail extends to larger z. In the representation of this tail by $n(z) \simeq z^{-\eta(T)}$ the parameter $\eta(T)$ decreases with decreasing T. Kosterlitz- Thouless theory predicts that in a 2D film $\eta(T)$ takes the value $\eta(T) = 0.25$ at T_c. That is, the superfluid onset temperature T_c in a 2D film can be obtained from the slope of the tail of the OBDM as the temperature at which $\eta(T)$ reaches 0.25. The function $n(z) = z^{-\eta(T)}$ for $\eta(T) = 0.25$ is shown as a black solid line in Fig. 14. If we adopt this criterion for confined ^{4}He using the OBDM shown in Fig. 14, we obtain the values of T_c (OBDM) listed in Table III. These are less accurate but agree well with the T_c obtained directly from $\rho_S(T)/\rho$. This agreement further supports the interpretation that the confined ^{4}He in nanopores for liquid radii in the range $6 \leqslant R \leqslant 11$ Å responds like a 2D fluid. It also shows that the $T_{\rm BEC}$ defined above lies above T_c, as observed in somewhat larger pore media [8,11,20–22,25].

Figure 15 (top) shows the OBDM of liquid ^{4}He confined to radius $R = 3$ Å. At short z along the pore $n(z)$ decreases approximately as a Gaussian. At larger z ($z \gtrsim 3$ Å), $n(z)$ decreases algebraically with z. There is little temperature dependence and no indication of a crossover to a constant $n(z)$ as in a 3D fluid. Superimposed on the algebraic decay of $n(z)$ are oscillations. An algebraically decaying $n(z)$ with oscillations at large z was predicted by Haldane [43] for a 1D fluid in the LL regime. The oscillations arise from the discrete nature of hard core bosons in 1D. The OBDM predicted by Haldane, valid at z large compared to the interatom spacing

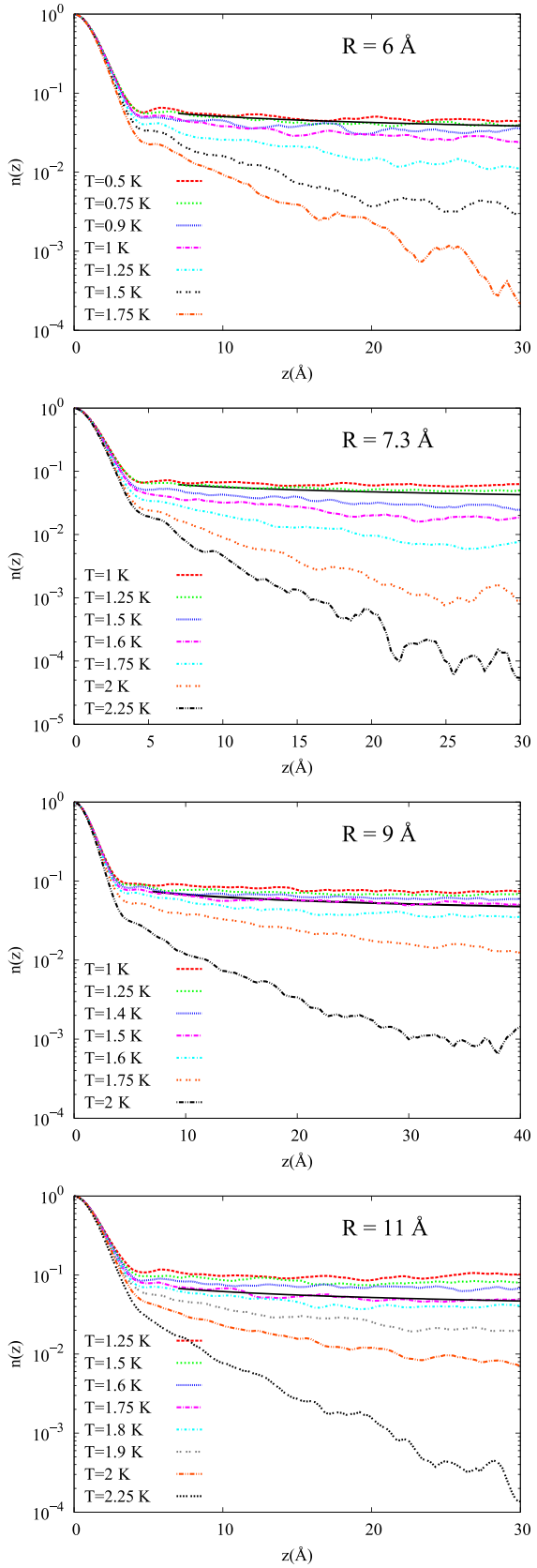

FIG. 14. (Color online) OBDM, $n(z)$, vs z along the pore at the temperatures indicated for liquid pore radii $R = 6$ Å to 11 Å (top to bottom). At $R = 11$ Å (pore diameter $d \simeq 32$ Å), a condensate fraction $n_0 \simeq 10\%$ at low temperature is indicated.

TABLE II. Onset temperature of BEC, $T_{\rm BEC}$, of liquid ^{4}He in smooth walled nanopores of liquid radius R (nanopore diameter $d = 2R + 10$ Å). The liquid is at SVP density and $T_{\rm BEC}$ is defined as the temperature at which the tail of the OBDM crosses over from exponential to algebraic decay.

R (Å)	d (Å)	$T_{\rm BEC}$ (K)
6	22	1.6
7.3	24.6	1.7
9	28	1.75
11	32	1.9

$[\rho_0{}^{-1} = (L/N)]$ and keeping only the lowest order ($m = 0,1$ terms), is

$$n(z) = \rho_0(\rho_0 z)^{-1/\eta}\left[B_0 + B_1\frac{1}{(\rho_0 z)^{\eta}}\cos(2\pi\rho_0 z)\right]. \quad (6)$$

The solid black line in Fig. 15 is a fit of Eq. (6) to the PIMC data at low temperature with ρ_0, B_0, B_1, and $\eta = 2K$ as adjustable parameters. The oscillations in the PIMC OBDM are well reproduced by this expression. This fit is discussed further in the Discussion section. The $n(z)$ at $R = 3$ Å is clearly characteristic of a 1D fluid.

Assuming translational invariance, the Luttinger liquid (LL) parameter for this 1D Bose fluid can also be expressed as [44,46] $K = (v_J/v_N)^{1/2}$, where $v_N = (\pi\hbar\rho_0^2)^{-1}\kappa_S^{-1}$ and κ_S is 1D compressibility of the Bose fluid, $\kappa_S^{-1} = L(d^2E/dL^2)$. This finally gives

$$K = \pi\hbar\left(\rho_0^3/m\right)^{\frac{1}{2}}\kappa_S^{\frac{1}{2}}. \quad (7)$$

Since $K^2 \propto \kappa_S$, K goes to ∞ for a noninteracting 1D Bose gas. For the Tonks gas $K = 1$. For a strongly interacting 1D Bose fluid with net attractive interactions [18,44,46], K can be $K < 1$. For the present 1D fluid at $R = 3$ Å, we find (1) $K = 0.35(3)$ from the fit to the OBDM in Fig. 15 (top) and (2) $K = 0.30(3)$ from a direct calculation of the compressibility (ground state energy) at $T = 1$ K and Eq. (7). These K values are mutually consistent.

For ^{4}He in a pore of radius $R = 2.9$ Å, Del Maestro *et al.* [15] find $K = 0.16$. Note that in Ref. [15] K^{-1} is used and $K^{-1} = 6.0$ is quoted. For liquid ^{4}He in a dislocation in solid ^{4}He, Boninsegni *et al.* [49] find $K^{-1} = 0.20(2)$.

TABLE III. Onset temperature for superflow, T_c, in liquid ^{4}He at SVP density in smooth walled nanopores of liquid pore radius R (nanopore diameter $d = 2R + 10$ Å) calculated from the PIMC superfluid density, $\rho_S(T)/\rho$, and the OBDM.

R (Å)	d (Å)	T_c [$\rho_S(T)/\rho$] (K)	T_c (OBDM) (K)
6	22	$\lesssim$0.5	$\sim$0.75
7.3	24.6	1.21(1)	$\sim$1.3
9	28	1.43(1)	1.4–1.5
11	32	1.74(1)	$\sim$1.75

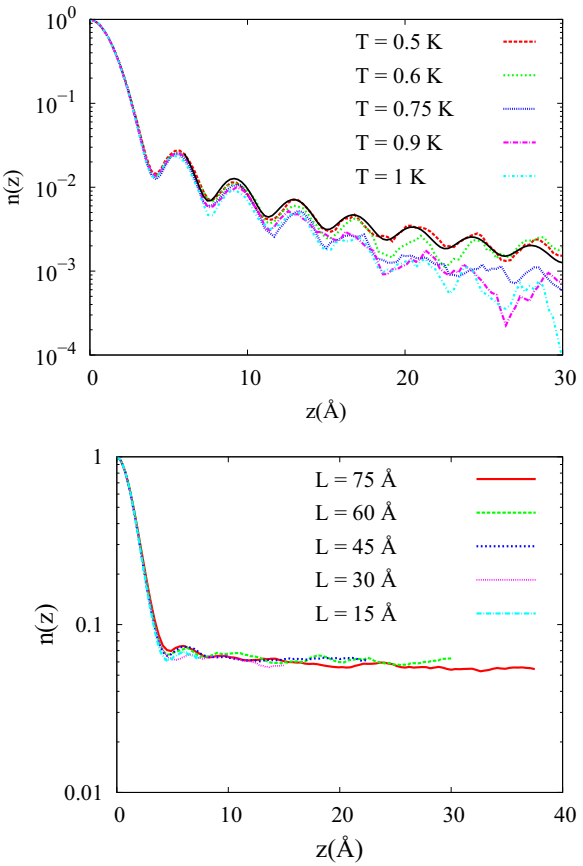

FIG. 15. (Color online) Top: OBDM, $n(z)$, vs z for $R = 3$ Å at several temperatures. The OBDM decays algebraically with z with oscillations at all temperatures. Bottom: OBDM vs z at low temperature for $R = 7.3$ Å and pore lengths $L = 15$–75 Å.

Finally, Fig. 15 (bottom) shows the tail of the OBDM as function of nanopore length L at liquid pore radius $R = 7.3$ Å, where the liquid shows 2D character. Within present statistical precision, we found that the the height and slope of the algebraic tail of $n(z)$ are independent of pore length for $L \geqslant 15$ Å.

At $R = 11$ Å, where the liquid shows some 3D character, the height of the tail (n_0) of the OBDM in Fig. 14 indicates a condensate fraction $n_0 \simeq 10\%$. This is comparable to but larger than the bulk liquid value at SVP, as observed [50] ($7.25\% \pm 0.75\%$) and calculated [33] with PIMC ($8.1\% \pm 0.2\%$ at 1 K). The density of the liquid in the pore at $R = 11$ Å ($\rho' = 0.191$ Å^{-3} from Table I) is smaller than the bulk value (0.0218 Å^{-3}), which is consistent with this difference. At $R = 7.3$ Å, an $n_0 \simeq 6\%$–7% is indicated if there is BEC.

IV. DISCUSSION

A. Effective dimensions of confined systems

The effective dimensions of a finite-sized system for thermal properties is generally determined by the ratio of the particle wavelength to the system size [18,19]. For ^{4}He in a nanopore this is the ratio of the ^{4}He atom thermal de Broglie wavelength $\lambda_T = [h^2/2\pi m k_B T]^{1/2}$ to the liquid pore diameter, $d_L = 2R$. If $\lambda_T > d_L$, the wavelength perpendicular to the pore is limited by d_L rather than set by λ_T. Perpendicular to the pore, the ^{4}He responds like a "particle in a box" and has discrete energy states. At low enough temperature the ^{4}He will remain in the ground state for the coordinates perpendicular to the pore and long wavelength excitations can be excited along the pore (1D) only. For thermal properties, the ^{4}He in the nanopore is one dimensional. Wada and collaborators [4,51] observe that the specific heat of liquid ^{4}He in 28 Å diameter FSM-16 crosses over from higher dimensions to 1D at low temperature confirming these arguments. A wide range of 1D systems has been discussed [18,19,46].

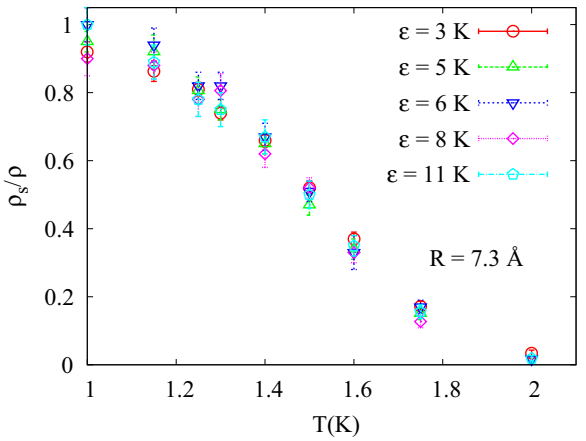

FIG. 16. (Color online) The superfluid fraction $\rho_S(T)/\rho$ as a function of the magnitude (ϵ) of the ^{4}He pore wall (attractive) potential. The $\rho_S(T)/\rho$ is insensitive to factor of 3 changes in magnitude of the attraction.

Superflow and BEC are, however, ground state as well as thermal properties. They can occur in the ground state. Different or additional criteria may determine the effective dimensions for these properties. The goal of the present paper is to determine the effective dimensions of liquid ^{4}He in nanopores for superflow and BEC from the scaling properties (1D, 2D, or 3D) of the ρ_S/ρ and of the long range behavior of the OBDM.

B. Model of liquid in a nanopore

A nanopore full of ^{4}He at SVP consists of (1) approximately 1.5–2 layers of inert (amorphous solid) helium adsorbed on the pore walls and (2) liquid ^{4}He in the interior of the pore. In FSM-16, the inert layers are estimated [6,12] to be 5 Å thick. The liquid is confined approximately to a cylinder of radius R in the center of the pore with $d = 2R + 10$ Å.

We have simulated only the cylinder of liquid in the interior. The inert layers and the nanopore itself were treated as a common material that confines the liquid to radius R. Physically the potential has a well-defined hard core whether it arises from helium or nanopore material. The confining potential is given by Eq. (2). The radius R of the liquid is set by the lower bound of the integration and the steepness of the repulsive core by σ. The magnitude of the attraction, set by ϵ, is not well known since it arises from a mix of helium and pore material. However, ρ_S/ρ is not sensitive to ϵ. Figure 16 shows that ρ_S/ρ changes little when ϵ is changed by a factor

of almost four. What is important is the hard wall radius, R, of the confining potential relative to the hard core diameter of the ^{4}He atom. This is a result familiar in bulk helium where a quite accurate condensate fraction of 9% (compared to the observed 7.25% $\pm$ 0.75%) can be obtained when helium is represented [52] by hard spheres without any attractive potential. Once R is selected, the liquid density N/V ($V = \pi R^2 L$) is set close to bulk density by choosing N (see Table I). Thereafter the ϵ was set to a reasonable value to ensure a liquid state in the interior but is otherwise not critical.

Any contribution to ρ_S/ρ passing through the inert layers is neglected in the present model. Given the absence of superflow [53] in solid ^{4}He and the existence of a critical filling (the inert layers) before superflow is observed in porous media [29], this appears to be a good approximation. The simulations in Refs. [15,16,32] showed a very small but not zero ρ_S/ρ in the inert layers.

C. Superfluidity and dimensions

For very small nanopores that have liquid pore radii $R =$ 3 Å (nanopore diameters $d = 2R + 10$ Å $= 16$ Å), we found that $\rho_S(T)/\rho$ scaled with T and pore length L as predicted by Luttinger liquid theory [14,15] for a 1D system. Specifically there is no static, zero frequency superflow. The apparent $\rho_S(T)/\rho$ is solely a finite-size effect and it goes to zero at $L = \infty$. At liquid pore radius $R = 3$ Å, it is not possible to fit two ^{4}He atoms (hard core diameter $\sigma \simeq 2.5$ Å) across the liquid. The ^{4}He lies at the center of the pore in a 1D line along the pore as shown in Fig. 11. The liquid is 1D.

For somewhat larger nanopores, $R = 4$ Å, it is possible for two ^{4}He atoms to lie across the liquid pore diameter R, as shown in Fig. 12. The cylindrical layer of ^{4}He has two "surfaces" (a minimum in density at the center of the pore and a minimum near the pore wall) as in a 2D layer. At $R = 4$ Å, the $\rho_S(T)/\rho$ no longer scales as a 1D LL. At larger R, in the range $6 \leqslant R \leqslant 11$ Å, the $\rho_S(T)/\rho$ scales as if it were a 2D system. For $4 \leqslant R \leqslant 11$ Å the liquid ^{4}He fills the nanopore effectively in 2D cylindrical layers as seen in Figs. 4 and 12. At these pore diameters, PIMC predicts a static, zero frequency ρ_S/ρ. The T_c is suppressed to a low value as shown in Table III. The low value arises from confinement alone with effects of disorder so far neglected. In this pore diameter range, the ρ_S/ρ goes to 1 at low temperature, as expected for straight, smooth walled nanopores with no disorder. Also, as seen in Fig. 7, there is significant finite-size broadening of $\rho_S(T)/\rho$ at higher temperature. This is also characteristic of 2D. For example in a flat, infinitely large 2D film, the $\rho_S(T)/\rho$ drops stepwise from a finite value to zero [54] at T_c. PIMC calculations [33] show substantial finite-size broadening of this transition in finite bulk films and T_c must, as here, be determined using scaling arguments. The $\rho_S(T)/\rho$ in 2D is further broadened in curved, finite-sized media [55–57] as found here.

At $R = 11$ Å ($d = 32$ Å), the $\rho_S(T)/\rho$ scales with T and pore length L equally well as a 2D or 3D fluid. At $R = 11$ Å the amplitude of the oscillations in the liquid density shown in Fig. 4 is significantly smaller. The liquid is approaching a uniform density as in a bulk 3D liquid. Also, the shape of $\rho_S(T)/\rho$ in the bottom frame of Fig. 7 is similar to that for 3D bulk liquid [33,58]. The magnitude of finite-size effects is much smaller in 3D. This suggests a crossover from 2D to 3D like liquid at or somewhat above $d = 32$ Å.

Extensive PIMC calculations of ρ_S/ρ of ^{4}He in nanopores have already been reported [14–16,32]. These extensive calculations include simulation of the inert layers as well as the liquid interior which is simulated here. The inert layers are found to be 5–6 Å thick (two layers) in agreement with experiment. Their contribution to the total ρ_S/ρ is very small but not zero. Nanopore diameters $20 \leqslant d \leqslant 30$ Å (liquid pore radii $5 \leqslant R \leqslant 10$ Å) were investigated. The focus was on the inner core. The $\rho_S(T)/\rho$ arising from the inner core of the density at all R investigated was found to scale following predictions of LL theory, as found here for $R = 3$ Å.

D. OBDM and dimensions

The top frame of Fig. 15 shows the OBDM for liquid ^{4}He confined to a liquid pore radius of $R = 3$ Å. At $z \gtrsim 3$ Å, the $n(z)$ shows oscillations superimposed on an algebraic tail as predicted by Eq. (6) for a 1D LL. The tail has little temperature dependence. The oscillations in $n(z)$ arise from the discrete nature [43] of the 1D hard core bosons. The period of the oscillations is set by the interatom spacing ($a = \rho_0^{-1} = L/N$) between the atoms in the 1D line, approximately 3.5 Å. The black solid line in Fig. 15 is a fit of Eq. (6) valid for $z \gg a$. The fit is clearly good which supports the interpretation of the OBDM as arising from a 1D fluid. Oscillations in the OBDM are not seen in 2D or 3D.

In contrast, the OBDMs for $4 \leqslant R \leqslant 11$ Å shown in Fig. 14 are characteristic of a 2D fluid. In $n(z)$ at large z there is a crossover from exponential decay at high temperature to algebraic decay at lower temperature. This crossover indicates the onset of algebraic off-diagonal long range order (AODLRO) as expected for a 2D fluid. At the lowest temperatures investigated and for $R = 11$ Å, $n(z)$ in Fig. 14 approaches a constant at large z as expected at $T = 0$ K in 2D and at all T below $T_{\rm BEC}$ in 3D.

The $T_{\rm BEC}$ in 3D fluids can be measured by observing [20,59] the temperature at which a long tail in $n(z)$ develops. The crossover from exponential to AODLRO can also be observed in 2D fluids [48]. We defined the $T_{\rm BEC}$ of liquid ^{4}He confined in nanopores as the temperature at which the tail of $n(z)$ crosses over from exponential to algebraic decay.

Finally, at $R = 11$ Å, the $\rho_S(T)/\rho$ scaled equally well as a 2D or 3D system. The OBDM at $R = 11$ Å similarly shows a mixed 2D/3D character. At low T the tail in $n(z)$ looks quite flat indicating BEC (3D). However at higher temperature (1.5–1.6 K), the decay is clearly algebraic (2D) whereas for a 3D system, for $T \leqslant T_{\rm BEC}$, $n(z)$ should be flat. Thus both the OBDM and $\rho_S(T)/\rho$ indicate a gradual crossover to 3D beginning at $R = 11$ Å ($d = 32$ Å).

E. Disorder

Nanopore walls can be rough and uneven. In order to assess the impact of rough walls we studied two simple models for $R = 7.3$ Å. First, we added $N_d = 50$ impurity particles randomly along the whole length of the $L = 30$ Å nanopore and separated from 7 to 9 Å from its axis. The N_d particles were fixed, interacting with He atoms via a simple

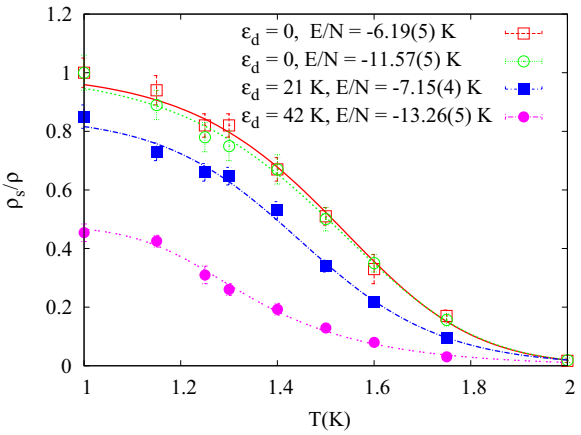

FIG. 17. (Color online) Superfluid fraction ρ_s/ρ vs T for $R = 7.3$ Å and for increasing disorder potential parameter ϵ_d. The results without disorder ($\epsilon_d = 0$) but with similar values of the energy per ^{4}He atom, E/N, for $T = 1$ K, are also shown for comparison.

Lennard-Jones potential with parameters ϵ_d and σ_d, thus creating an additional static external potential. The impurity potential creates random pockets of stronger attraction. We took $\sigma_d = 2$ Å and performed the simulation for several ϵ_d values keeping the ϵ in the confining He-nanopore interaction, given by Eq. (2), fixed at 3 K. Figure 17 shows $\rho_S(T)/\rho$ for $\epsilon_d = 0$ (no disorder), $\epsilon_d = 21$ K, and $\epsilon_d = 42$ K. The superfluid fraction clearly decreases with increasing impurity interaction strength ϵ_d. The energy per ^{4}He atom, E/N, also decreases with increasing ϵ_d. To normalize for the decreased E/N, we increased the ϵ in the confining potential to $\epsilon = 6$ K and 11 K to obtain $\rho_S(T)/\rho$ for similar E/N values but without disorder ($\epsilon_d = 0$). Figure 17 shows that $\rho_S(T)/\rho$ is quite insensitive to ϵ and E/N without disorder. This is in strong contrast to the marked decrease in $\rho_S(T)/\rho$ with disorder.

In a second model we have added 16 or 30 N_d particles per $L = 30$ Å length of nanopore in a 6 Å long strip. This way we created necks along the pore every 30 Å where there are narrower attractive pockets. Our preliminary results indicate that the superfluidity is even more suppressed in this case for similar values of ϵ_d. In addition, the ρ_s/ρ vs T curves for $L = 30$ Å and $L = 60$ Å cross at a lower temperatures than observed in the model without disorder.

These exploratory calculations suggest that if nanopore inhomogeneity is taken into account the superfluid fraction is further suppressed and the transition moved to slightly lower temperatures, in accordance with the experimental findings. Further calculations are in progress.

F. Comparison with experiment

Ikegami *et al.* [60] and Wada *et al.* [6] report extensive measurements of $\rho_S(T)/\rho$ in FSM-16 nanopores of diameter $d = 15$, 18, 22, 24, 28, and 47 Å. Similarly, Taniguchi *et al.* [10–12] report $\rho_S(T)/\rho$ in FSM-16 at $d = 28$ Å including its pressure dependence as shown in Fig. 1. Both Wada *et al.* [6] and Taniguchi *et al.* [12] find that the first 1.5 layers of ^{4}He on the pore walls (5 Å thick) are inert and do not contribute to superflow. The cylinder of liquid in the interior of FSM-16 corresponding to the diameters d above therefore has radius $R = 2.5$, 4, 6, 9, and 18.5 Å.

At $R = 2.5$ Å ($d = 15$ Å), no superflow ($\rho_S/\rho = 0$) is observed [6,60]. In agreement, the present PIMC predicts no superflow and 1D Luttinger liquid at $R = 3$ Å. At $R = 4$ Å a superfluid fraction is observed [6,60]. PIMC similarly predicts a finite ρ_S/ρ at $R = 4$ Å. PIMC also predicts a pronounced crossover from 1D to a 2D layer filling in the nanopores between 3 Å and 4 Å. This good agreement suggests that only at very small pore diameters, $d \leqslant 16$ Å, does ^{4}He behave like a 1D fluid in nanopores (as far as superfluidity is concerned). At $d \geqslant 18$ Å the liquid behaves more like a 2D (layered) liquid. Similarly, the agreement suggests that the superflow observed at $d \geqslant 18$ Å is genuine static 2D superflow (observable at zero oscillation frequency) as calculated in PIMC. There could be in addition some frequency dependent effects. PIMC predicts a zero frequency ρ_S/ρ.

In small diameter nanopores, the superfluid onset temperature, T_c, is suppressed to low temperatures. Ikegami *et al.* [60] and Wada *et al.* [6] report $T_c \simeq 1$ K in FSM-16, Taniguchi *et al.* [11] $T_c = 0.9$ K in $d = 28$ Å FSM-16, and Yamamoto *et al.* [7] $T_c = 1.4$ K in 25 Å gelsil, all at SVP. The observed T_c decreases still further with increasing pressure [7,11] (see Fig. 1). From Table III, PIMC predicts a $T_c = 1.2$ K at $d = 25$ Å at SVP, in approximate agreement with observed values. At smaller diameters, the T_c predicted by PIMC drops rapidly from 1.0 to 0.5 K. As seen in Fig. 6, the PIMC T_c decreases with increasing density (pressure). The PIMC results for smooth walled nanopores without disorder are thus in good agreement with experiment.

The present agreement suggests, first, that the low observed values of T_c can be reproduced by static superflow as calculated by PIMC. That is, the transition to static (2D) superflow can take place at low temperature in nanopores. A frequency dependent theory [13] in which there is no actual static superflow (as in 1D) is not needed to explain the low observed values of T_c. Second, the physical reason for the low T_c values is that the confined liquid responds like a 2D fluid. The T_c in (infinite) films [33] of liquid ^{4}He is $T_c = 0.653 \pm 0.010$ K for density $\rho = 0.0432$ Å^{-2}. Thus if liquid ^{4}He in nanopores responds like layers of 2D liquid, we can expect a major drop in T_c as d is reduced simply from the crossover of dimensions from 3D to 2D. The crossover from 3D to 2D behavior of the liquid within conventional 2D superfluidity [47,54,61] provides a straightforward explanation of the low values of T_c in smaller diameter nanopores.

BEC in ^{4}He at SVP in MCM-41 ($d = 47$ Å) and Vycor ($d \simeq 70$ Å) has been observed [20,62]. In MCM-41, the observed [20] condensate fraction at $T = 0$ K is $n_0(0) = 3.3\% \pm 0.40\%$. Given that roughly 45% in the ^{4}He is in the inert layers, this translates to $n_0(0) \simeq 6\%$ in the liquid. The present PIMC $n_0(0) \simeq 10\%$ at $d = 32$ Å is consistent with this given that the PIMC density is somewhat below the SVP liquid density (see Table I). The BEC onset temperature in MCM-41 is $T_{\rm BEC} = T_\lambda = 2.17$ K, the bulk value within precision. At $d = 32$ Å PIMC predicts $T_{\rm BEC} = 1.9$ K with $T_{\rm BEC}$ increasing with increasing pore diameter (see Table II). Extrapolation of PIMC values suggests a PIMC $T_{\rm BEC} = T_\lambda$ at $d = 47$ Å. Both

the observed and PIMC $T_{\rm BEC}$ lie well above the $T_c = 1.58$ K observed in MCM-41 [20].

V. CONCLUSION

PIMC calculations of the superfluid fraction, $\rho_S(T)/\rho$, and the OBDM, $n(z)$, in liquid ^{4}He in nanopores of diameter $16 \leqslant d \leqslant 32$ Å have been made. Only the liquid in the pores was simulated with the inert ^{4}He layers on the pore walls assumed totally inert. At very small pore diameter, $d \leqslant 16$ Å, the $\rho_S(T)/\rho$ and $n(z)$ scale like a 1D Luttinger liquid. At $d = 16$ Å, the liquid is confined to a single line of atomic dimensions in the center of the pore. There is a crossover to 2D behavior at $d = 18$ Å. In the range $18 \leqslant d \leqslant 32$ Å, PIMC predicts a zero frequency $\rho_S(T)/\rho$ that scales as in a 2D fluid with a low T_c and a $n(z)$ that decays algebraically at large z. The superflow is standard, static superfluidity in 2D. The T_c obtained from the OBDM via Kosterlitz-Thouless theory is consistent with the T_c obtained from ρ_S/ρ. In this d range, the liquid is deposited in the nanopore in 2D-like layers. Many experiments explore this diameter range [4–12]. The T_c observed is low. The present results reproduce this low T_c because PIMC predicts the liquid is 2D and T_c is low in 2D. The PIMC T_c decreases with increasing density as is observed [7,9–12]. At $d = 32$ Å the $\rho_S(T)/\rho$ scales equally well as a 2D or 3D liquid and T_c is higher. It is anticipated that at $d \geqslant 32$ Å the confined liquid will respond like a 3D liquid with a higher T_c. Our exploratory calculations indicate that nanopore inhomogeneity leads to reduction of the superfluid fraction and the transition temperature. It would be therefore most interesting to explore further effects of rough pore walls and a disordered potential in the present model.

ACKNOWLEDGMENTS

The authors gratefully acknowledge Massimo Boninsegni for providing the PIMC code used in this work and Marcus Holtzmann for valuable discussions and insights on reduced-dimensional systems and phase transitions. H.R.G. thanks the Theory Group, Institut Laue-Langevin, where part of this paper was written, for hospitality. L.V.M. acknowledges support from the Fulbright program.

[1] J. D. Reppy, J. Low Temp. Phys. **87**, 205 (1992).
[2] M. H. W. Chan, K. I. Blum, S. Q. Murphy, G. K. S. Wong, and J. D. Reppy, Phys. Rev. Lett. **61**, 1950 (1988).
[3] K. Huang and H. F. Meng, Phys. Rev. B **48**, 6687 (1993).
[4] N. Wada, J. Taniguchi, H. Ikegami, S. Inagaki, and Y. Fukushima, Phys. Rev. Lett. **86**, 4322 (2001).
[5] N. Wada, Y. Minato, T. Matsushita, and M. Hieda, J. Phys. Soc. Jpn. **77**, 111012 (2008).
[6] N. Wada, Y. Minato, T. Matsushita, and M. Hieda, J. Low Temp. Phys. **162**, 549 (2011).
[7] K. Yamamoto, H. Nakashima, Y. Shibayama, and K. Shirahama, Phys. Rev. Lett. **93**, 075302 (2004).
[8] K. Yamamoto, Y. Shibayama, and K. Shirahama, Phys. Rev. Lett. **100**, 195301 (2008).
[9] J. Taniguchi and M. Suzuki, J. Low Temp. Phys. **150**, 347 (2008).
[10] J. Taniguchi, Y. Aoki, and M. Suzuki, Phys. Rev. B **82**, 104509 (2010).
[11] J. Taniguchi, R. Fujii, and M. Suzuki, Phys. Rev. B **84**, 134511 (2011).
[12] J. Taniguchi, K. Demura, and M. Suzuki, Phys. Rev. B **88**, 014502 (2013).
[13] T. Eggel, M. A. Cazalilla, and M. Oshikawa, Phys. Rev. Lett. **107**, 275302 (2011).
[14] A. Del Maestro and I. Affleck, Phys. Rev. B **82**, 060515 (2010).
[15] A. Del Maestro, M. Boninsegni, and I. Affleck, Phys. Rev. Lett. **106**, 105303 (2011).
[16] B. Kulchytskyy, G. Gervais, and A. Del Maestro, Phys. Rev. B **88**, 064512 (2013).
[17] A. Kotani, K. Yamashita, and D. S. Hirashima, Phys. Rev. B **83**, 174515 (2011).
[18] M. A. Cazalilla, R. Citro, T. Giamarchi, E. Orignac, and M. Rigol, Rev. Mod. Phys. **83**, 1405 (2011).
[19] A. Imambekov, T. L. Schmidt, and L. I. Glazman, Rev. Mod. Phys. **84**, 1253 (2012).
[20] S. O. Diallo, R. T. Azuah, D. L. Abernathy, J. Taniguchi, M. Suzuki, J. Bossy, N. Mulders, and H. R. Glyde, Phys. Rev. Lett. **113**, 215302 (2014).
[21] H. R. Glyde, O. Plantevin, B. Fak, G. Coddens, P. S. Danielson, and H. Schober, Phys. Rev. Lett. **84**, 2646 (2000).
[22] O. Plantevin, H. R. Glyde, B. Fåk, J. Bossy, F. Albergamo, N. Mulders, and H. Schober, Phys. Rev. B **65**, 224505 (2002).
[23] F. Albergamo, H. R. Glyde, D. R. Daughton, N. Mulders, J. Bossy, and H. Schober, Phys. Rev. B **69**, 014514 (2004).
[24] J. V. Pearce, S. O. Diallo, H. R. Glyde, R. T. Azuah, T. Arnold, and J. Z. Larese, J. Phys.: Condens. Matter **16**, 4391 (2004).
[25] J. Bossy, J. Ollivier, H. Schober, and H. R. Glyde, Europhys. Lett. **98**, 56008 (2012).
[26] H. R. Glyde and W. G. Stirling, in *Phonons 89*, edited by S. Hunklinger, W. Ludwig, and G. Weiss (World Scientific, Singapore, 1990).
[27] F. Albergamo, J. Bossy, P. Averbuch, H. Schober, and H. R. Glyde, Phys. Rev. Lett. **92**, 235301 (2004).
[28] J. Bossy, T. Hansen, and H. R. Glyde, Phys. Rev. B **81**, 184507 (2010).
[29] G. A. Csáthy, J. D. Reppy, and M. H. W. Chan, Phys. Rev. Lett. **91**, 235301 (2003).
[30] R. A. Aziz, F. R. McCourt, and C. C. K. Wong, Mol. Phys. **61**, 1487 (1987).
[31] G. J. Tjatjopoulos, D. L. Feke, and J. A. Mann, J. Phys. Chem. **92**, 4006 (1988).
[32] A. Del Maestro, Int. J. Mod. Phys. B **26**, 1244002 (2012).
[33] M. Boninsegni, N. V. Prokof'ev, and B. V. Svistunov, Phys. Rev. Lett. **96**, 070601 (2006).
[34] M. Boninsegni, N. V. Prokof'ev, and B. V. Svistunov, Phys. Rev. E **74**, 036701 (2006).
[35] B. E. Clements, J. L. Epstein, E. Krotscheck, and M. Saarela, Phys. Rev. B **48**, 7450 (1993).
[36] M. Rossi, D. E. Galli, and L. Reatto, Phys. Rev. B **72**, 064516 (2005).
[37] E. S. Hernndez, J. Low Temp. Phys. **162**, 583 (2011).
[38] E. L. Pollock and D. M. Ceperley, Phys. Rev. B **36**, 8343 (1987).
[39] D. M. Ceperley and E. L. Pollock, Phys. Rev. B **39**, 2084 (1989).

[40] V. Privman (ed.), *Finite Size Scaling and Numerical Simulation of Statistical Systems* (World Scientific, Singapore, 1990).
[41] E. L. Pollock and K. J. Runge, Phys. Rev. B **46**, 3535 (1992).
[42] J. K. Perron, M. O. Kimball, K. P. Mooney, and F. M. Gasparini, Phys. Rev. B **87**, 094507 (2013).
[43] F. D. M. Haldane, Phys. Rev. Lett. **47**, 1840 (1981).
[44] M. A. Cazalilla, J. Phys. B **37**, S1 (2004).
[45] J. M. Luttinger, J. Math. Phys. **4**, 1154 (1963).
[46] T. Giamarchi, *Quantum Physics in One Dimension* (Oxford University Press, Oxford, 2004).
[47] J. M. Kosterlitz and D. J. Thouless, J. Phys. C: Solid State Phys. **6**, 1181 (1973).
[48] S. O. Diallo, J. V. Pearce, R. T. Azuah, J. W. Taylor, and H. R. Glyde, Phys. Rev. B **78**, 024512 (2008).
[49] M. Boninsegni, A. B. Kuklov, L. Pollet, N. V. Prokof'ev, B. V. Svistunov, and M. Troyer, Phys. Rev. Lett. **99**, 035301 (2007).
[50] H. R. Glyde, R. T. Azuah, and W. G. Stirling, Phys. Rev. B **62**, 14337 (2000).
[51] N. Wada, T. Matsushita, M. Hieda, and R. Toda, J. Low Temp. Phys. **157**, 324 (2009).
[52] M. H. Kalos, D. Lesque and L. Verlet, Phys. Rev. A **9**, 2178 (1974).
[53] D. Y. Kim and M. H. W. Chan, Phys. Rev. Lett. **109**, 155301 (2012).
[54] D. R. Nelson and J. M. Kosterlitz, Phys. Rev. Lett. **39**, 1201 (1977).
[55] V. Kotsubo and G. A. Williams, Phys. Rev. B **33**, 6106 (1986).
[56] J. Machta and R. A. Guyer, Phys. Rev. Lett. **60**, 2054 (1988).
[57] T. Minoguchi and Y. Nagaoka, Prog. Theor. Phys. **80**, 397 (1988).
[58] J. S. Brooks, B. B. Sabo, P. C. Schubert, and W. Zimmermann, Jr., Phys. Rev. B **19**, 4524 (1979).
[59] H. R. Glyde, S. O. Diallo, R. T. Azuah, O. Kirichek, and J. W. Taylor, Phys. Rev. B **83**, 100507 (2011).
[60] H. Ikegami, Y. Yamato, T. Okuno, J. Taniguchi, N. Wada, S. Inagaki, and Y. Fukushima, Phys. Rev. B **76**, 144503 (2007).
[61] D. J. Bishop and J. D. Reppy, Phys. Rev. Lett. **40**, 1727 (1978).
[62] R. T. Azuah and collaborators (private communication).